



OPEN ACCESS

EDITED BY

Felix Sharipov,
Federal University of Paraná, Brazil

REVIEWED BY

Noreen Sher Akbar,
National University of Sciences and
Technology (NUST), Pakistan
Ebenezer Bonyah,
University of Education, Winneba, Ghana

*CORRESPONDENCE

Sayed M. Eldin,
✉ sayed.eldin22@fue.edu.eg
Anwar Saeed,
✉ anwarsaeed769@gmail.com

SPECIALTY SECTION

This article was submitted
to Fluid Dynamics,
a section of the journal
Frontiers in Physics

RECEIVED 30 January 2023

ACCEPTED 20 March 2023

PUBLISHED 07 April 2023

CITATION

Faizan Ahmed M, Khalid M, Ali F,
Al-Bossly A, Alduais FS, Eldin SM and
Saeed A (2023), Importance of
bioconvection flow on tangent
hyperbolic nanofluid with
entropy minimization.
Front. Phys. 11:1154478.
doi: 10.3389/fphy.2023.1154478

COPYRIGHT

© 2023 Faizan Ahmed, Khalid, Ali, Al-Bossly, Alduais, Eldin and Saeed. This is an open-access article distributed under the terms of the [Creative Commons Attribution License \(CC BY\)](https://creativecommons.org/licenses/by/4.0/). The use, distribution or reproduction in other forums is permitted, provided the original author(s) and the copyright owner(s) are credited and that the original publication in this journal is cited, in accordance with accepted academic practice. No use, distribution or reproduction is permitted which does not comply with these terms.

Importance of bioconvection flow on tangent hyperbolic nanofluid with entropy minimization

M. Faizan Ahmed¹, M. Khalid¹, Farhan Ali¹, Afrah Al-Bossly²,
Fuad S. Alduais², Sayed M. Eldin^{3*} and Anwar Saeed^{4*}

¹Department of Mathematical Sciences, Federal Urdu University of Arts, Sciences & Technology, Karachi, Pakistan, ²Department of Mathematics, College of Science and Humanities in Al-Kharj, Prince Sattam Bin Abdulaziz University, Al-Kharj, Saudi Arabia, ³Center of Research, Faculty of Engineering, Future University in Egypt New Cairo, New Cairo, Egypt, ⁴Department of Mathematics, Abdul Wali Khan University, Mardan, Khyber Pakhtunkhwa, Pakistan

The amalgamation of microorganisms in the nanofluid is significant in beautifying the thermal conductivity of several systems, such as microfluid devices, chip-shaped microdevices, and enzyme biosensors. The current investigation studies mixed convective flow of the entropy minimization of unsteady MHD tangent hyperbolic nanoliquid because a stretching surface has motile density *via* convective and slip conditions. For the novelty of this work, the variable transport characteristics caused by dynamic viscosity, thermal conductivity, nanoparticle mass permeability, and microbial organism diffusivity are considered. It is considered that the vertical sheet studying the flow. By using the appropriate alteration, the governing equations for the most recent flow analysis were altered into a non-dimension relation. Through MATLAB Software *bvp4c*, the PDE model equations have been made for these transformed equations. Engineering-relevant quantities against various physical variables include force friction, Nusselt number, Sherwood number, and microorganism profiles. The results showed good consistency compared to the current literature. Moreover, these outcomes revealed that augmentation in the magnitude of the magnetic field and velocity slip parameter declines the velocity profile. The reverse impact is studied in *We*. In addition, heat transfer is typically improved by the influence of thermal radiation parameters, Brownian movement, and thermophoretic force. The physical interpretation has existed through graphical and tabular explanations.

KEYWORDS

nanofluids, entropy minimization, gyrotactic microorganism, MHD, thermal radiation

1 Introduction

A passion sparked by the study of non-Newtonian fluids in recent decades. Several researchers have various features in the technological, chemical, and mechanical industries. The most convenient applications to encounter non-Newtonian fluids like polymeric relation, atomic reactor, solvent, biomedical in tumor, and many more. Because of the complexity of their design and subsequent management according to the model of power kind, non-Newtonian fluids can produce a connection between shear stress and shear rate that is non-linear. Because of the complexity of these fluids, it is not possible to understand the rheological properties of fluids of this type using a straightforward relation, in contrast to the Newtonian fluid. In order to determine the nature of these occurrences, the researchers

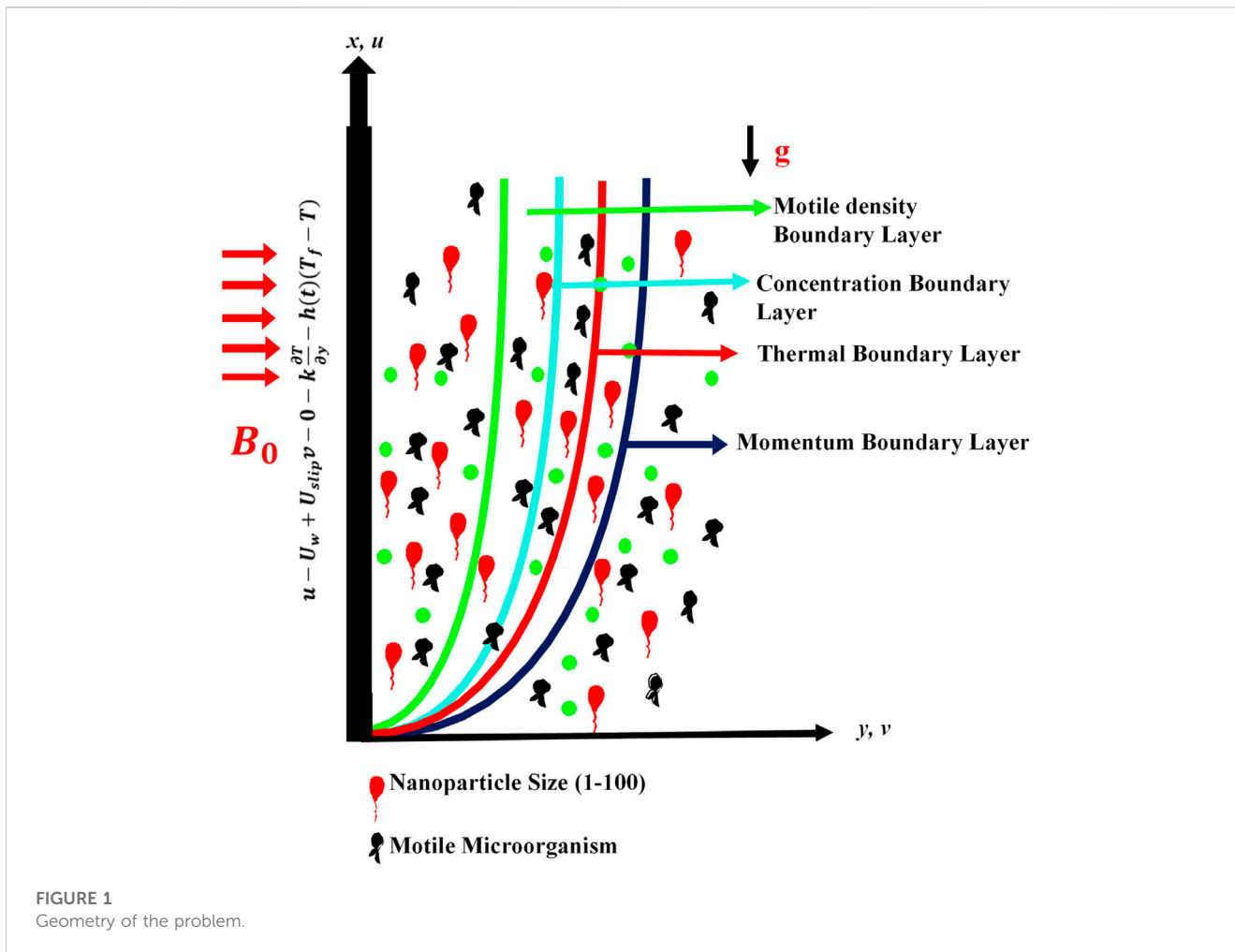
offered a number of mathematical studies to investigate the material associated with non-Newtonian fluids. The tangent hyperbolic fluid model illustrates a model in which an increase in the shear effect reduces the effective viscosity of the fluid. References [1, 2] first described the flow of tangent hyperbolic fluid in a boundary layer caused by a stretched sheet. Hayat et al. [3] described the boundary-layer flow of tangent hyperbolic fluid under mass flux conditions. The double solution of tangent hyperbolic was probed by Nagendramma et al. [4]. The effect of convective conditions on tangent hyperbolic fluid induced by the homogenous–heterogeneous reaction was completed by Kumar et al. [5]. The bioconvection flow of tangent hyperbolic due to a movable surface using numerical methods was completed by Kamel et al. [6]. The effect of numerical analysis of the bioconvection flow on the tangent hyperbolic fluid past Riga plate was scrutinized by Waqas et al. [7]. The impact of the zero mass flux condition for the tangent hyperbolic nanoparticles past an exponential surface due to statistical analysis was found by Shafiq et al. [8]. The unsteady flow on the tangent hyperbolic fluid past a wedge surface was conducted by Ali et al. [9]. Hussain et al. [10] scrutinized the unsteady flow of permeable surfaces for the tangent hyperbolic fluid under slip conditions. Shafiq et al. proposed the influence of Newtonian heating having microorganisms on tangent hyperbolic nanofluid [11]. Ramzan et al. presented the 3D tangent hyperbolic nanofluid of the heat flux theory with activation energy [12].

According to experts, nanoliquid is the most innovative and compelling technology currently used in engineering and technological products, including cooling agents, vehicles, catalyst reactions, and computer chips. The thermophysical characteristics of a nanoliquid are more important than those of a regular liquid. The presence of the nanoparticle in the regular fluid is investigated for potential effects on the fluid's thermophysical characteristics. Choi [13] created the main invention in this field. The Williamson nanofluid due to the permeable surface was done by Bhatti and Rashidi [14]. Hayat et al. [15] described the melting heat transfer with thermal radiation induced by the variable thickness of the carbon nanotubes (CNT). Kumar et al. studied the effect of semiconductors on the thermal properties of CuO-H₂O with the base fluid of nanoparticles [16]. The influence of thermal radiation using Sisko nanofluid with activation energy was evaluated by Ijaz et al. [17]. Khan and Shehzad [18] investigated the joule heating effect for the flow of third-grade nanomaterials due to the periodic motion sheet. The induction of nanoparticles in solar energy was discussed by Fayaz et al. [19]. Faizan et al. [20] examined how fluids move thermally and generate entropy during the tangent hyperbolic flow with the Darcy–Forchheimer flow across a stretching surface. Olanrewaju et al. [21] exploited Maxwell nanofluid due to the permeable surface by second law analysis. The heat transfer in the porous surface for the second law analysis of Maxwell nanofluid was reported by Alagumalai et al. [22], elaborating on applying nanofluid with thermal energy and technological applications. Tayebi et al. [23] discovered the natural convection flow of nanofluids with entropy generation due to annular enclosure. Chamka et al. [24] constituted an MHD natural convection flow and thermal radiation in the cavity enclosure using the finite element method. Seyyedi et al. [25] examined the MHD natural convection flow of nanofluids on entropy minimization in a wavy porous enclosure. Dogonchi et al. [26] explained the combined effect of

thermal radiation and joule heat on the natural convection of nanoliquid between two disks. Eshaghi et al. [27] discussed the Baffle length H-shaped cavity with the addition of nanoparticles. Afshar et al. [28] probed the free convection flow of nanofluids inside the porous wavy enclosure. A titanium dioxide nanofluid based on 10 W40 subjected to electroosmotic forces and peristaltic propulsion in a curved microchannel is the subject of the current study, which focuses on the fluid flow analysis and heat transfer properties of the material explored by Akram et al. [29]. Maraj et al. [30] analyzed the oscillatory pressure-driven MHD flow of a hybrid nanofluid in a vertical rotating channel with velocity slip, thermal periodic limitations, and the effect of hall current, which are the main topics of the current mathematical investigation. Akram et al. [31] investigated the fluid flow properties and heat transmission by the drilling muds augmented with nanoparticles flowing through the drilling pipes under different physical conditions. Shah et al. [32] investigated how energy is transferred as engine oil-based Prandtl–Eyring nanofluid flows across a heated stretching surface. The influence of slip velocity across a vertically declining sheet, heat generation and absorption, and convection in a two-dimensional magnetic nanofluid are all statistically investigated by Asghar et al. [33]. Some other important studies can be found [34–39].

Researchers have used the oxytactic and erratic motion of microorganisms as a model to examine the processes of bioconvection. Slanting swimming cells are related to bioconvection, which focuses on different types of microorganisms. Ecological systems, biofuels, biosensors, and many more technologies successfully use the physical meaning of bioconvection. Due to the interaction of microorganisms, the bioconvection of nanoparticles is correlated with density. It has been noted that gyrotactic bacteria successfully increased the stability of nanoparticles. In recent years, several researchers have examined significant events. The effect of bioconvection employing nanoparticles past a permeable sheet was studied by Saini and Sharma [40]. Dhanai et al. [41] investigated the MHD flow gyrotactic microorganism on the nanoparticles past an inclined sheet. The force connection with bioconvection resulting from a vertical wedge plate was performed by Mahdy [42]. Avinash et al. [43] found the magnetic field of natural convective and microorganisms together with nanoliquid. Makinde and Animasaun [44] analyzed the impact of non-linear thermal radiation induced by the microorganism with a magnetic field and nanofluid. The impact of the slip effect with MHD flow on gyrotactic microorganisms was conducted by Khan et al. [45]. The mixed convective flow of bioconvection past a spongy plate was designed by Mutuku and Makinde [46]. The impact of convective conditions on the magnetic field flow of bioconvection was worked on by Khan et al. [47].

It has been brought to our attention that the second law analysis of bioconvection phenomena in the flow of tangent hyperbolic nanofluids with a slip effect under thermal radiation has not yet been considered. The motive is to fill the gap. This was discovered after careful observation of the review highlighted previously. In contrast to the standard approach, the flow, in this case, is caused by a vertical surface. It has been thoroughly reviewed and determined that such characteristics are not researched. Fluid flow past vertical stretching sheets has been proven to have numerous applications in



current times due to physical and technological applications, such as the processing of polymers, the petrochemical sector, various production processes, glass production, and rolling hot. Because of these motivating factors, we decided to direct our attention to this substantial research gap. The present investigation was performed by simulating the features of thermal radiation, which has studied a large variety of features in thermal extrusion processing, solar energy, defense system, heavy automatic equipment, atomic chain reactions, and many other processes. The answer to the inserted problem is approached by methodically computing it using the BVP4c approach. The graphical results of various emerging variables besides the flow field are studied and evaluated.

2 Problem formulation

We presume a two-dimensional, laminar, unsteady, velocity effect of an MHD incompressible tangent hyperbolic nanofluid comprising bioconvection with entropy analysis. The fluid system is surrounded by a stretched sheet that is saturated with motile microorganisms and has a velocity of $U_w(x, t) = \frac{cx}{1-ct}$ along the (\bar{x}) direction. Magnetic fields and stretched sheets are perpendicular to one another, whereby the induced magnetic field is ignored by the

truly low magnetic Reynolds number (Figure 1). The Roseland approximation can be used to anticipate the radiation effect because the fluid is considered optically thick. Furthermore, it is assumed that the temperature of the fluid T_w on the sheet is higher than the temperature T_∞ in the free stream. The mathematical formulation in this study employs the Cartesian coordinate. The impacts of Brownian motion, thermophoresis, and convective effects are used to examine the heat, concentration, and motile density of the transit rates of microorganisms. The flow phenomena are described using the following equations.

The constitutive equation for the flow of the model (continuity, momentum, energy, concentration, and microorganism) is represented as follows [48–53]:

$$\frac{\partial u}{\partial \bar{x}} + \frac{\partial v}{\partial \bar{y}} = 0, \frac{\partial u}{\partial t} + u \frac{\partial u}{\partial \bar{x}} + v \frac{\partial u}{\partial \bar{y}} = \nu(1-n) \frac{\partial^2 u}{\partial \bar{y}^2} + \sqrt{2} \nu m \Gamma \left(\frac{\partial u}{\partial \bar{y}} \right) \left(\frac{\partial^2 u}{\partial \bar{y}^2} \right) - \frac{\sigma B_0^2}{\rho} u + \tag{1}$$

$$g\beta(1 - C_\infty)(T - T_\infty) - g \left(\frac{\rho_p - \rho_f}{\rho_f} \right) (C - C_\infty) - \gamma_1 g \left(\frac{\rho_m - \rho_f}{\rho_f} \right) (N - N_\infty), \tag{2}$$

$$\frac{\partial T}{\partial t} + u \frac{\partial T}{\partial x} + v \frac{\partial T}{\partial y} - \tau \left\{ D_B \left(\frac{\partial C}{\partial y} \frac{\partial T}{\partial y} \right) + \frac{D_T}{T_\infty} \left(\frac{\partial T}{\partial y} \right)^2 \right\} = \left(\alpha_f + \frac{16\sigma T_\infty^3}{3k_f(\rho c_p)_f} \right) \frac{\partial^2 T}{\partial y^2}, \tag{3}$$

$$\frac{\partial C}{\partial t} + u \frac{\partial C}{\partial x} + v \frac{\partial C}{\partial y} = D_B \left(\frac{\partial^2 C}{\partial y^2} \right) + \left(\frac{D_T}{T_\infty} \right) \left(\frac{\partial^2 T}{\partial y^2} \right) - k_\infty (C - C_\infty), \tag{4}$$

$$\frac{\partial N}{\partial t} + u \frac{\partial N}{\partial x} + v \frac{\partial N}{\partial y} + b \frac{W_c}{C_\infty} \frac{\partial}{\partial y} \left(N \frac{\partial C}{\partial y} \right) = D_m \frac{\partial^2 N}{\partial y^2}. \tag{5}$$

The corresponding boundary conditions are

$$\left. \begin{aligned} u &= U_w + U_{slip}, v = 0, -k \frac{\partial T}{\partial y} = h(t)(T_f - T), C = C_w, \chi = \chi_w \text{ at } y = 0 \\ u &\rightarrow 0, T \rightarrow T_\infty, C \rightarrow C_\infty, \chi \rightarrow \chi_\infty \text{ as } y \rightarrow \infty \end{aligned} \right\}. \tag{6}$$

Here, the component of velocity is (u, v) in the direction of (x, y) , volume expansion of the fluid is β , stretching velocity is U_w , gravity of the fluid is g , heat transfer coefficient is $h(t)$, thermophoretic diffusion is D_T , Brownian movement is D_B , microorganism diffusivity is D_m , specific heat is C_p , kinematic viscosity is ν , electric conductivity of the nanofluid is σ , temperature of the fluid is T , density of the nanofluid is ρ_f , swimming speed cell is W_c , density of the nanomaterial is ρ_p , the density of microorganism particles is ρ_m , ambient temperature is T_∞ , ambient concentration is C_∞ , and ambient microorganism concentration is N_∞ .

By considering the appropriate transformation [20],

$$\left. \begin{aligned} \eta &= y \sqrt{\frac{c}{v(1-\epsilon t)}}, \psi = x \sqrt{\frac{cv}{(1-\epsilon t)}} f(\eta), u = \frac{cx}{(1-\epsilon t)} f'(\eta), h(t) = \frac{d}{\sqrt{(1-\epsilon t)}} \\ v &= -\sqrt{\frac{cv}{(1-\epsilon t)}} f(\eta), \theta(\eta) = \frac{T - T_\infty}{T_w - T_\infty}, \phi(\eta) = \frac{C - C_\infty}{C_w - C_\infty}, \chi = \frac{N - N_\infty}{N_w - N_\infty} \end{aligned} \right\}. \tag{7}$$

The application of the suitable alteration in Eqs 2–5, subject to the boundary conditions in Eq. 6, is rendered into a system of ODEs [48]:

$$(1-n)f''' + nWe f'' f''' - (f')^2 + \lambda(\theta - Nr\phi - Rb\chi) - A \left(f' + \frac{\eta}{2} f'' \right) - M f' = 0, \tag{8}$$

$$\theta'' \left(1 + \frac{4}{3} Rd \right) + Pr \left(f\theta' - \frac{\eta}{2} A\theta' + Nb\theta'\phi' + Nt\theta'^2 \right) = 0, \tag{9}$$

$$\phi'' + Sc f\phi' - \frac{\eta}{2} Sc A\phi' + \frac{Nt}{Nb} \theta'' - \kappa\phi = 0, \tag{10}$$

$$\chi'' - Pe\phi'' + f\chi' + \phi'\chi' - Lb \left(\frac{1}{2} \eta Sc A\chi' \right) = 0. \tag{11}$$

The boundary conditions are as follows [20], [42], [48]:

$$\left. \begin{aligned} f(0) &= 0, f'(0) - 1 - \Upsilon f''(0) = 0, \theta' + Bi(1 - \theta(0)) = 0, \chi(0) = 1 \\ f'(\infty) &= 0, \theta(\infty) \rightarrow 0, \phi(\infty) \rightarrow 0, \chi(\infty) \rightarrow 0 \end{aligned} \right\}. \tag{12}$$

The dimensionless variables in the aforementioned equations are the unsteady parameter denoted by A , Weissenberg number denoted by We , magnetic number denoted by M , Brownian motion denoted by Nb , thermophoretic parameter denoted by

Nt , Schmidt number denoted by Sc , Peclet number denoted by Pe , bioconvection Lewis number denoted by Lb , Biot number denoted by Bi , heat capacity ratio of the nanofluid denoted by τ , Prandtl number denoted by Pr , microorganism concentration difference denoted by ω , mixed convection parameter denoted by λ , bouncy force denoted by Nr , and bioconvection Rayleigh number denoted by Rb :

$$\left. \begin{aligned} A &= \left(\frac{\epsilon}{C} \right), We = \left(\frac{\sqrt{2a^3} \Gamma U}{\sqrt{\nu}} \right), M = \left(\frac{\sigma B_c^2}{\rho a} \right) \\ N_b &= \left(\frac{\tau D_B (C_w - C_\infty)}{\nu} \right), N_t = \left(\frac{\tau D_T (T_w - T_\infty)}{\nu} \right), \\ Sc &= \left(\frac{\nu}{D_B} \right), Pe = \left(\frac{bWe}{D_m} \right), L_b = \left(\frac{\nu_f}{D_m} \right), \\ Bi &= \left(\frac{h}{k} \sqrt{\frac{\nu(1-\epsilon t)}{a}} \right), \tau = \left(\frac{(\rho_c)_p}{(\rho_c)_f} \right), \\ Pr &= \left(\frac{\nu}{\alpha_f} \right), \omega = \left(\frac{N_\infty}{N_f - N_\infty} \right), \lambda = \left(\frac{Gr}{Re_x^2} \right), \\ Nr &= \left(\frac{g\beta_c (C_w - C_\infty)}{g\beta_T (T_w - T_\infty)} \right), Rb = \left(\frac{\gamma_1 (\rho_m - \rho_f) (N_w - N_\infty)}{\rho_f \beta (1 - C_\infty) (T_w - T_\infty)} \right). \end{aligned} \right\} \tag{13}$$

Skin friction, Nusselt number, Sherwood number, and motile microorganism are as follows:

$$\left. \begin{aligned} C_f &= \frac{2\tau_w}{\rho u_w^2}, \\ Nu_x &= \frac{xq_w}{k(T_w - T_\infty)}, \\ Sh_x &= \frac{xq_m}{D_B(T_w - T_\infty)}, \\ Nn_x &= \frac{xq_n}{D_m(N_w - N_\infty)}. \end{aligned} \right\} \tag{14}$$

The values for the aforementioned quantities are as follows:

$$\left. \begin{aligned} \tau_w &= \mu \left((1-n) \frac{\partial u}{\partial y} + 2\Gamma n \left(\frac{\partial u}{\partial y} \right)^2 \right), \\ q_w &= \frac{\partial T}{\partial y} \Big|_{y=0}, \\ q_m &= \frac{\partial C}{\partial y} \Big|_{y=0}, \\ q_N &= \frac{\partial N}{\partial y} \Big|_{y=0}. \end{aligned} \right\} \tag{15}$$

Equation 14 and Eq. 15 by using Eq. 7

$$\left. \begin{aligned} C_f Re_x^{0.5} &= \left((1-n)f''(0) + \frac{n}{2} We f''(0)^2 \right), \\ \frac{Nu_x}{Re_x^{0.5}} &= -\theta'(0), \\ \frac{Sh_x}{Re_x^{0.5}} &= -\phi'(0), \\ \frac{Nn_x}{Re_x^{0.5}} &= -\chi'(0). \end{aligned} \right\} \tag{16}$$

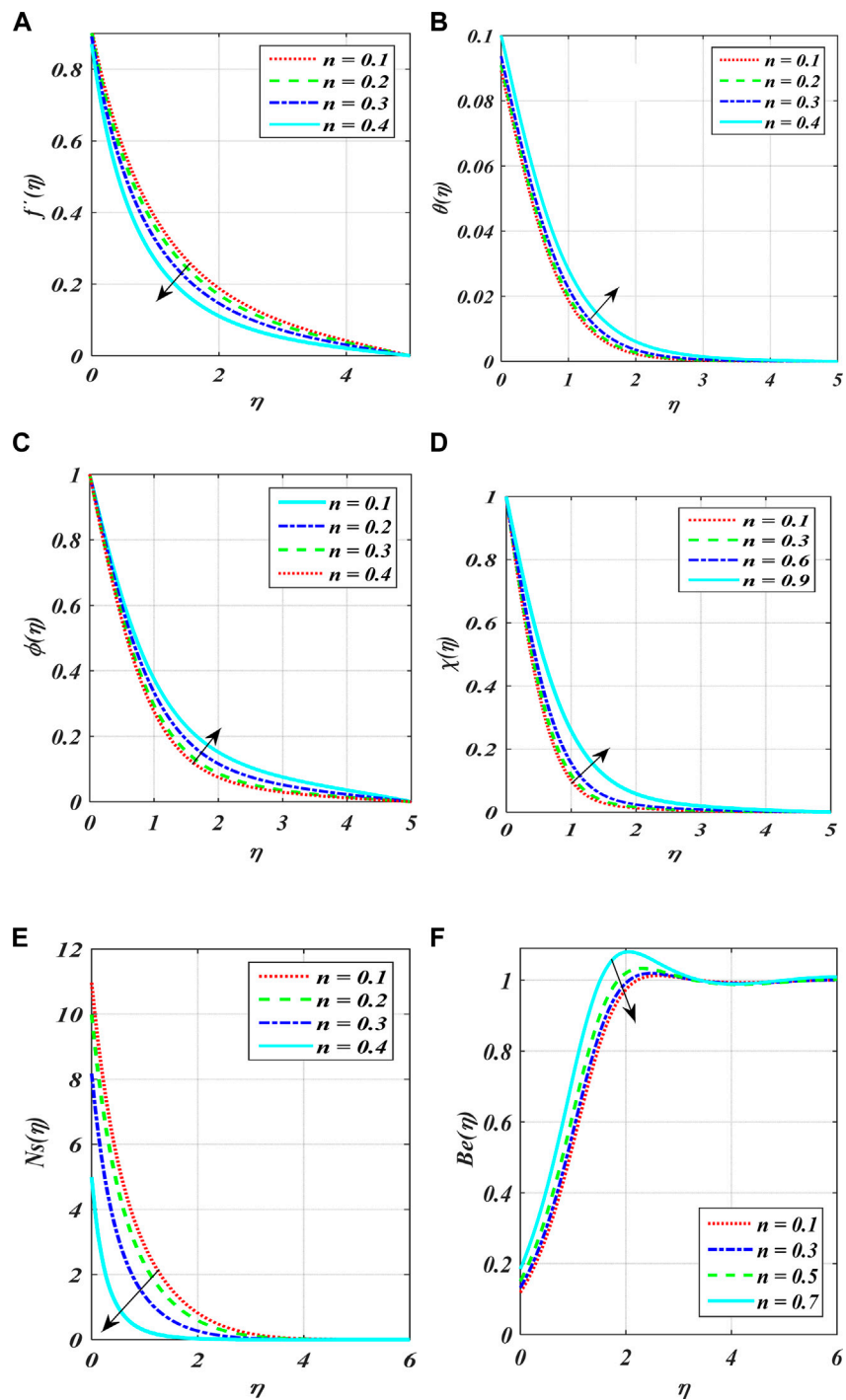
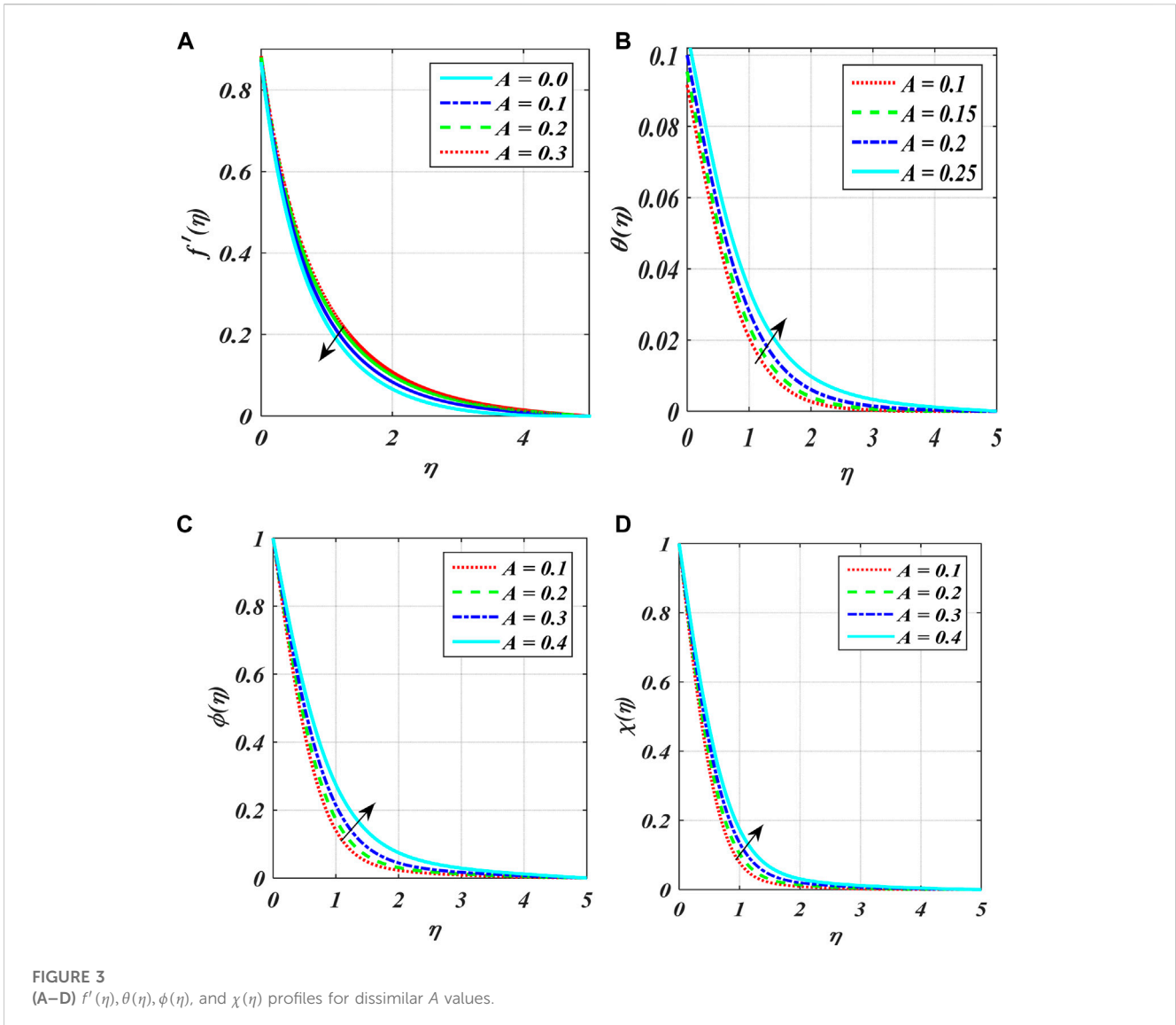


FIGURE 2 (A–F) $f'(\eta)$, $\theta(\eta)$, $\phi(\eta)$, $\chi(\eta)$, $Ns(\eta)$, and $Be(\eta)$ profiles for dissimilar n values.

3 Implemented strategy

It is obvious that the presented problem Eqs. (8–11) with boundary assumptions Eq. 12 cannot be handled analytically due to the problem’s extreme non-linearity. Hence, we employ the well-known BVP4c technique to simulate the numerical solution.

Actually, BVP4c is used as a powerful method to achieve accurate results. The ordinary differential boundary value problem is resolved using this method. Each method, such as bvp4c MATLAB, has advantages and disadvantages. The main advantage is that it accepts multipoint BVPs natively, in contrast to many other solvers. As the source code is public,



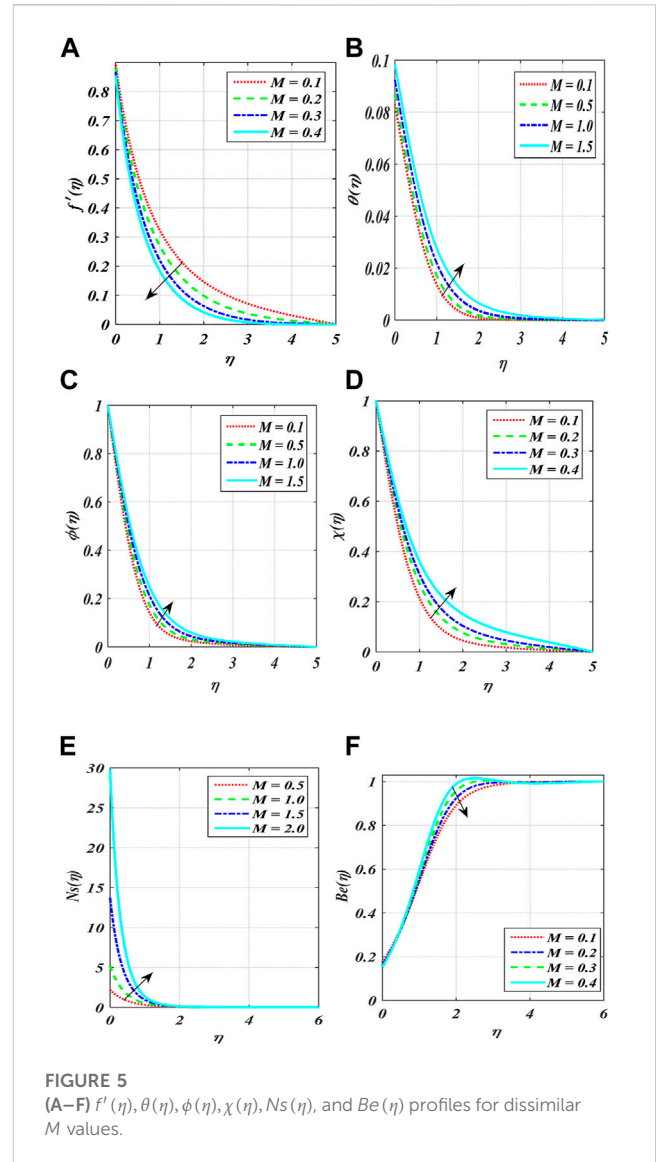
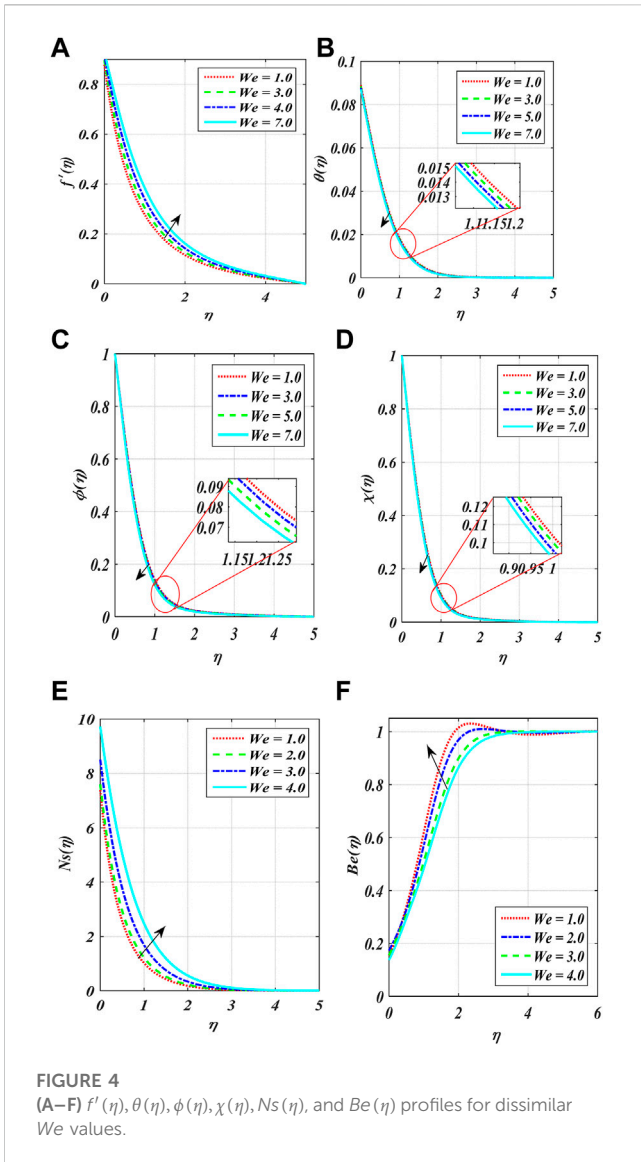
we can easily and gratis modify it to function with already-existing equations. MATLAB is an interpreted language; thus, making corrections is easy. Moreover, there are several issues concerning its ability to resolve first-order differential equations. You must first reduce your system to the first order before utilizing the bvp4c MATLAB method to solve higher orders. MATLAB executes more slowly than C and C++ because, as was already mentioned, it is an interpreted language. The technique turns the initial BVP into an IVP by applying the following presumptions: we will assign a few extra variables to accomplish this goal:

$$\left(\begin{matrix} f = R_1 \\ f' = R_2 \\ f'' = R_3 \\ f''' = \dot{R}_3 \end{matrix} \right) \left(\begin{matrix} \theta = R_4 \\ \theta' = R_5 \\ \theta'' = \dot{R}_5 \end{matrix} \right) \left(\begin{matrix} \phi = R_6 \\ \phi' = R_7 \\ \phi'' = \dot{R}_7 \end{matrix} \right) \left(\begin{matrix} \chi = R_8 \\ \chi' = R_9 \\ \chi'' = \dot{R}_9 \end{matrix} \right), \quad (17)$$

$$\left. \begin{aligned} \dot{R}_3 &= \frac{A\left(R_2 + \frac{\eta}{2}R_3\right) + (R_2)^2 - R_1R_3 + MR_2 - \lambda(R_4 - NrR_6 - RbR_8)}{(1-n) + eWeR_3} \\ \dot{R}_5 &= -Pr\left(R_1R_5 - \frac{\eta}{2}AR_5 + NtR_5R_7 + Nt(R_5)^2\right) \\ \dot{R}_7 &= \frac{\eta}{2}AScR_7 - ScR_1R_7 + \frac{Nt}{Nb}\left(Pr\left(R_1R_5 - \frac{\eta}{2}AR_5 + NtR_5R_7 + Nt(R_5)^2\right)\right) \\ \dot{R}_9 &= Lb\left(\frac{\eta}{2}ScAR_9\right) - R_7R_9 - R_1R_9 + Pe\left(\frac{\eta}{2}AScR_7 - ScR_1R_7 + \frac{Nt}{Nb}\left(Pr\left(R_1R_5 - \frac{\eta}{2}AR_5 + NtR_5R_7 + Nt(R_5)^2\right)\right)\right) \end{aligned} \right\}. \quad (18)$$

The criteria for new variable boundaries include

$$\left. \begin{aligned} R_1(0) = 0, R_2(0) = 1 + YR_3(0), R_5(0) = -Bi(1 - R_4(0)), R_8(0) = 1 \\ R_2(\infty) = 0, R_4(\infty) = 0, R_6(\infty) = 0, R_8(\infty) = 0 \end{aligned} \right\}. \quad (19)$$



The far boundary is $\eta \rightarrow \infty$; we put it by $\eta = 5$ (for different distributions). The method produces consistent and quick convergence throughout the extensive deviation of calculating parameters. We utilized the step size of 0.001 and continued to perform this method until the parameters for the tolerance level were reached 10^{-6} .

4 Entropy generation

The influence of the magnetic field, thermal radiation and diffusion, and entropy generation S_G for the tangent hyperbolic nanofluid is given by [54]

$$\begin{aligned}
 S_G = & \frac{k}{T_\infty} \left(1 + \frac{16\sigma^* T_\infty^3}{3kk^*} \right) \left(\frac{\partial T}{\partial y} \right)^2 + \frac{\mu}{T_\infty} \left(\frac{\partial u}{\partial y} \right)^2 \left[(1-n) + \frac{n\Gamma}{\sqrt{2}} \frac{\partial u}{\partial y} \right] \\
 & + \frac{RD_m}{C_\infty} \left(\frac{\partial C}{\partial y} \right)^2 + \frac{RD_m}{T_\infty} \left(\frac{\partial T}{\partial y} \right) \left(\frac{\partial C}{\partial y} \right) + \frac{RD_m}{\chi_\infty} \left(\frac{\partial N}{\partial y} \right)^2 \\
 & + \frac{RD_m}{T_\infty} \left(\frac{\partial N}{\partial y} \right) \left(\frac{\partial T}{\partial y} \right) + \frac{\sigma B_0^2}{T_\infty} u^2.
 \end{aligned}
 \tag{20}$$

Eq. 20 shows the formation of entropy through the first phrase, which represents heat transfer, the second term, fluid friction, and the third term through the sixth term, diffusive irreversibility. The importance of entropy production can be expressed mathematically as

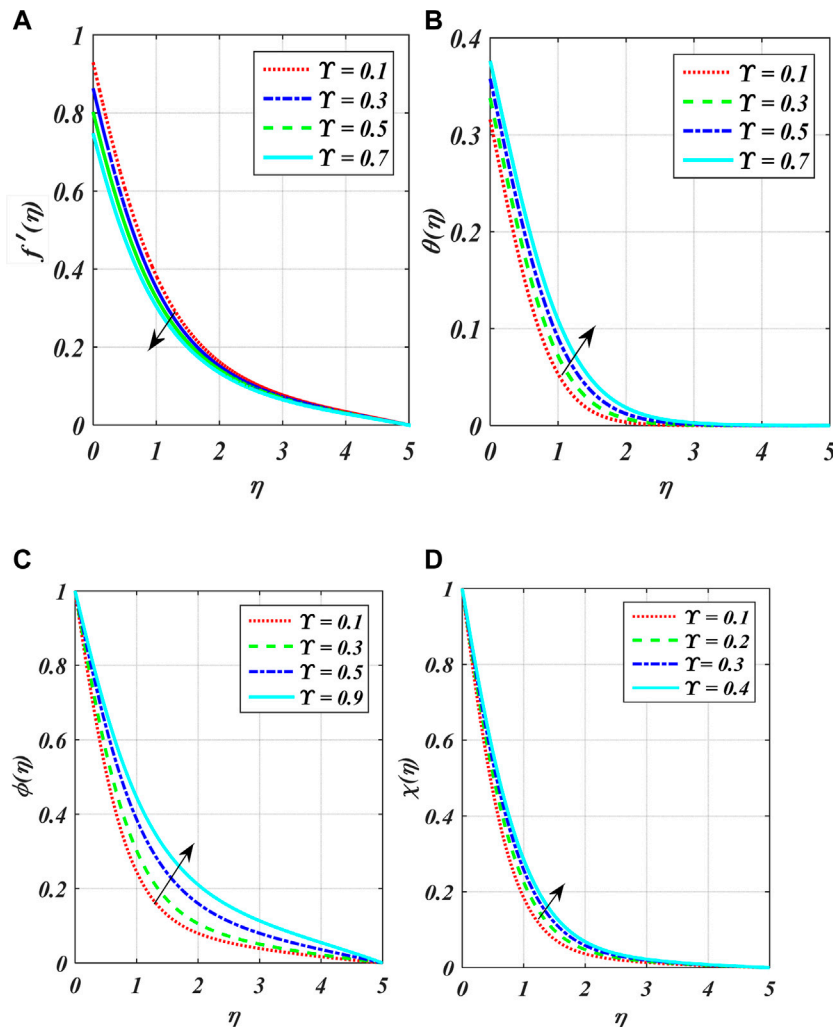


FIGURE 6 (A–D) $f'(\eta)$, $\theta(\eta)$, $\phi(\eta)$, and $\chi(\eta)$ profiles for dissimilar Υ values.

$$S_o^m = \frac{\kappa(\Delta T)^2}{L^2 T_\infty^2} \tag{21}$$

Using Eq. 6, it is possible to modify the rate of entropy minimization using tangent hyperbolic [54]:

$$N_s = \frac{S_G}{S_{G_o}} = (1 + Rd)\theta'^2 + Re_x \frac{Br}{\Pi} [(1 - n)f''^2] + \frac{nWe^2}{2} \frac{Br}{\Pi} Re_x f'''^3 + Re_x \left(\frac{\Gamma}{\Pi}\right)^2 \phi'^2 + Re_x \left(\frac{\Gamma}{\Pi}\right) \phi' \theta' + Re_x \left(\frac{\xi}{\Pi}\right)^2 \chi'^2 + Re_x \left(\frac{\xi}{\Pi}\right) \chi' \theta' + \frac{Br}{\Pi} M f'^2, \tag{22}$$

$$Be = \frac{\text{Entropy due to heat transfer}}{\text{Total entropy}}, \tag{23}$$

$$Be = \frac{(1 + Rd)\theta'^2 + Re_x \left(\frac{\Gamma}{\Pi}\right)^2 \phi'^2 + Re_x \left(\frac{\Gamma}{\Pi}\right) \phi' \theta' + Re_x \left(\frac{\xi}{\Pi}\right)^2 \chi'^2 + Re_x \left(\frac{\xi}{\Pi}\right) \chi' \theta' + \frac{Br}{\Pi} M f'^2}{(1 + Rd)\theta'^2 + Re_x \frac{Br}{\Pi} [(1 - n)f''^2] + \frac{nWe^2}{2} \frac{Br}{\Pi} Re_x f'''^3 + Re_x \left(\frac{\Gamma}{\Pi}\right)^2 \phi'^2 + Re_x \left(\frac{\Gamma}{\Pi}\right) \phi' \theta' + Re_x \left(\frac{\xi}{\Pi}\right)^2 \chi'^2 + Re_x \left(\frac{\xi}{\Pi}\right) \chi' \theta' + \frac{Br}{\Pi} M f'^2}. \tag{24}$$

5 Result and discussion

The numerous variables over $f'(\eta), \theta(\eta), \phi(\eta), \chi(\eta), N_s(\eta), Be(\eta)$ are elaborated in Figures 2–10. It has been noted that each flow variable has remained constant throughout the procedure, such as $M = 0.4, Nr = 0.1, Rb = 0.7, Lb = 0.2, Pe = 1.2, We = 1.1, n = 1.0, A = 0.2, Pr = Sc = 1.0, Nb = Nt = 0.4$. This section describes the behavior of each of the physical parameters. Figures 2A–F show the variation of n on velocity profile $f'(\eta)$, temperature field $\theta(\eta)$, concentration $\phi(\eta)$, motile density profiles, $\chi(\eta)$ entropy production $Ns(\eta)$, and Bejan number $Be(\eta)$.

Figures 2A–F show the variation in power index number n over $f'(\eta), \theta(\eta), \phi(\eta), \chi(\eta), Ns(\eta)$, and $Be(\eta)$. It is clear from depreciating in $f'(\eta)$ with the larger value of n . Physically, the fluid’s viscosity, or its thickness, is determined by this characteristic. For small values of n , the fluid exhibits shear thinning characteristics; for larger values of n , shear thickening; and for $n = 1$, Newtonian characteristics. When n is larger than one, the fluid’s velocity slows down, producing a weaker velocity field. The

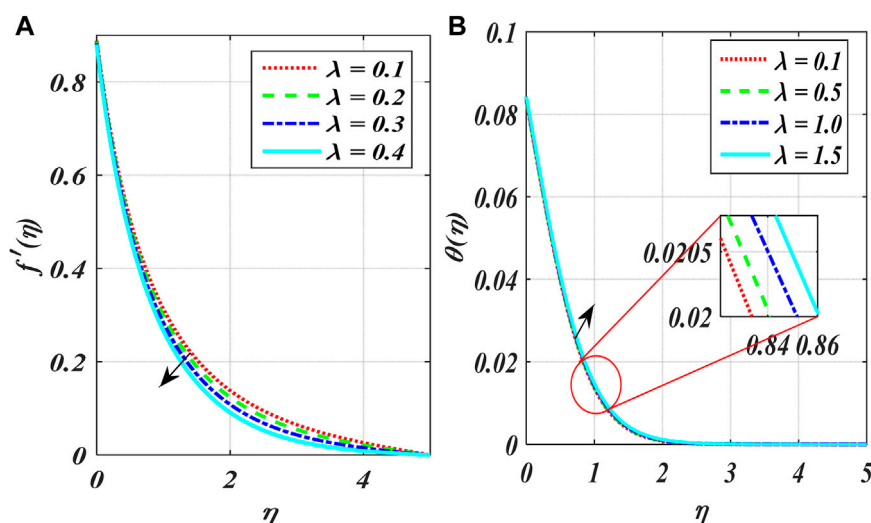


FIGURE 7 (A,B) $f'(\eta)$ and $\theta(\eta)$ profiles for dissimilar λ values.

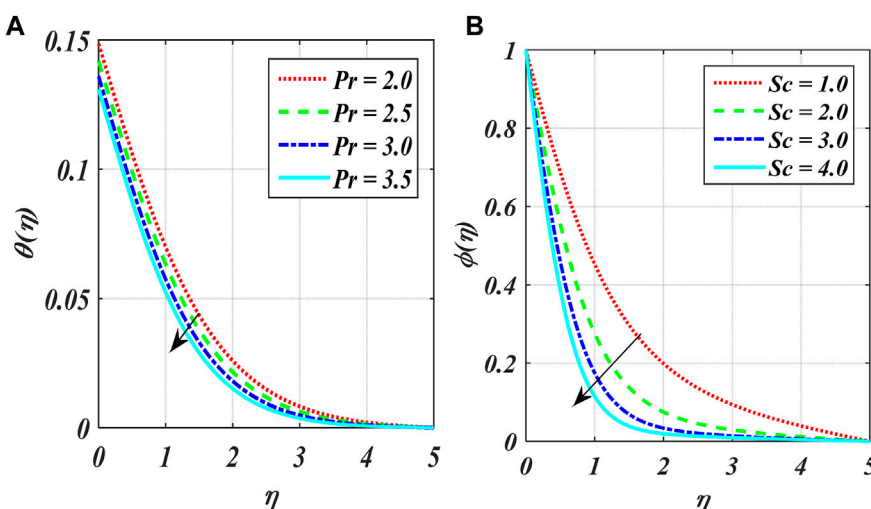


FIGURE 8 (A,B) $\theta(\eta)$ and $\phi(\eta)$ profiles for dissimilar Pr and Sc values.

thermal layer field $\theta(\eta)$, concentration of nanoparticles $\phi(\eta)$, and motile density profiles $\chi(\eta)$ are shown in Figures 2B–D. The thermal field $\theta(\eta)$ and corresponding layer thickness have been improved for the bigger magnitude of n . In essence, the described model becomes more sophisticated as the power-law index rises. With the development of this component, the fluid’s non-Newtonian properties steadily get worse. As a result, the velocity’s diminishing tendency can be explained. Figures 2C, D show concentration $\phi(\eta)$ and motile density profiles $\chi(\eta)$ and exhibit observable similarities in their behavior. With an increase in the power-law coefficient n , the fluid becomes more viscous. As a result, the concentration and motile density profile improve gradually. Figures 2E, F present the influence of n on $Ns(\eta)$ and $Be(\eta)$ profile. It is reported that with the increase in n values, the entropy

generation increased significantly, whereas the Bejan number fell considerably. Figures 3A–D show the A over velocity curve $f'(\eta)$, temperature field $\theta(\eta)$, concentration $\phi(\eta)$, and motile density profiles $\chi(\eta)$. Figure 3A shows that the velocity distribution $f'(\eta)$ has been minimized to achieve a more accurate assessment of A . Actually, the slower pace of the stretched sheet allows the fluid to cool down. As a result, the fluid’s particles settle down, and the system’s heat is released. The effect is that fluid viscosity also gradually increases. As a result, as can be seen in the image, the profile gradually decreases as the unsteadiness parameter’s values rise. The increase in the value of A induces an acceleration in all three profiles—thermal $\theta(\eta)$, concentration $\phi(\eta)$, and motile density $\chi(\eta)$ —as shown in Figures 3B–D. An increase in the unsteady parameter A results in an increase in the kinetic energy

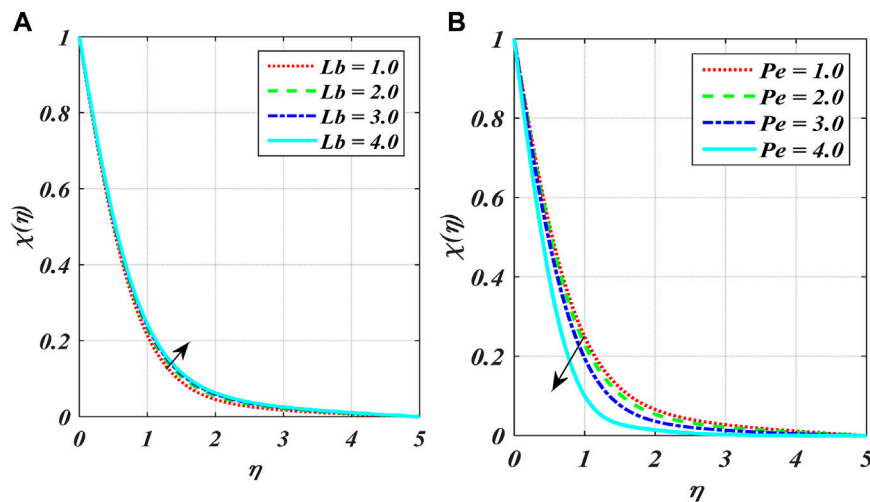
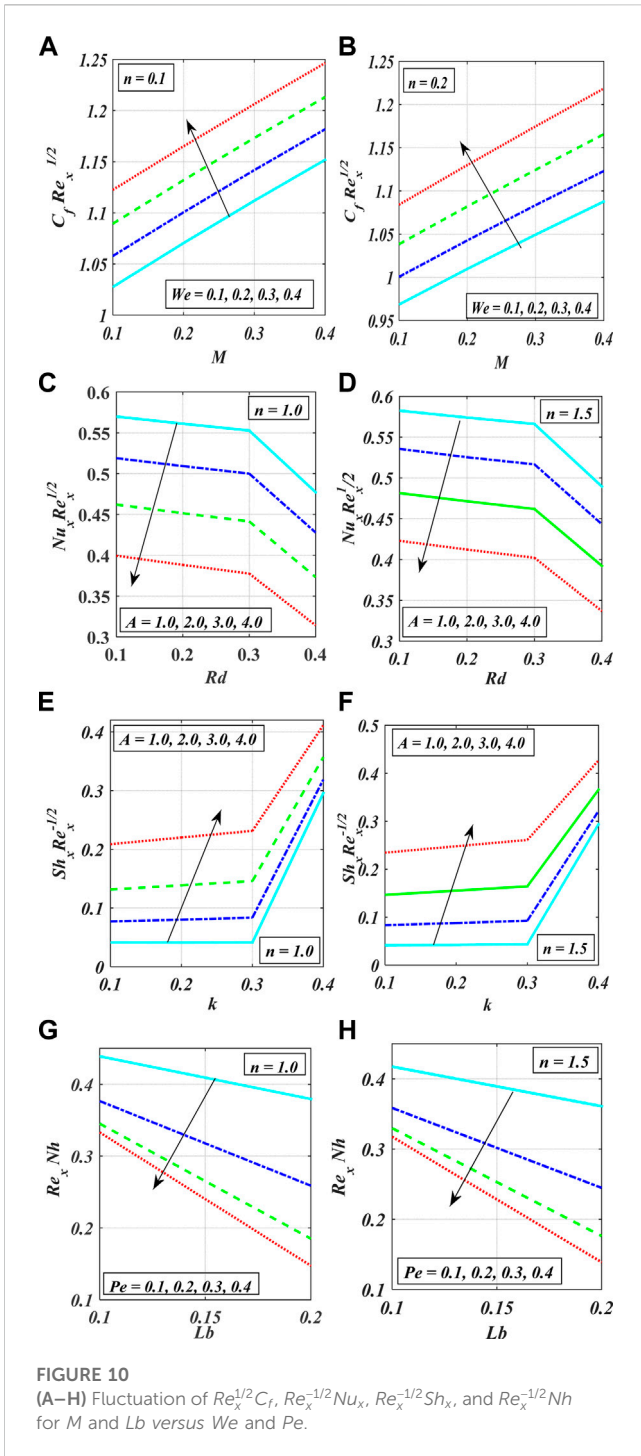


FIGURE 9
(A,B) $\chi(\eta)$ profiles for dissimilar Lb and Pe values.

of the fluid, which increases the motion of the liquid film. Figures 4A–F show fluctuation of We on velocity profile $f'(\eta)$, temperature field $\theta(\eta)$, concentration $\phi(\eta)$, motile density profiles $\chi(\eta)$, entropy production $Ns(\eta)$, and Bejan number $Be(\eta)$. When applied to the flow field, We reflects the fraction of the time scale corresponding to the actual time. Accordingly, the increase in We improves the velocity profile $f'(\eta)$ shown in Figure 4A. Actually, the movement of fluid slowly decreases with the Weissenberg number. Moreover, We is the proportion of relaxation time and other process time due to this relaxation time depreciating the fluid velocity increase with We . Figures 4B–D show the temperature field $\theta(\eta)$, concentration $\phi(\eta)$, and motile density profiles $\chi(\eta)$ diminished with a larger value of We . The Weissenberg number influence on entropy generation and Bejan number are revealed in Figures 4E, F. For larger, We the $Ns(\eta)$ and $Be(\eta)$ enhances. Physically, for higher We , more heat is lost because of relaxation time and more resistance between fluid particles, which is the reason $Ns(\eta)$ and $Be(\eta)$ increase. Figures 5A–F show the performance of M for velocity profiles $f'(\eta)$, temperature fields $\theta(\eta)$, concentrations $\phi(\eta)$, motile density profiles $\chi(\eta)$, entropy production $Ns(\eta)$, and the Bejan number $Be(\eta)$. For larger magnitudes of the magnetic field M , it is obvious that the velocity profile $f'(\eta)$ will decrease due to an increase in the magnetic field's strength. When $M = 0$, the flow is hydrodynamic, and when $M \neq 0$, the flow is magnetic. Actually, the decrease in velocities is caused by the resistive force of the magnetic field, which is always normal to an electrically conducting fluid flow. The Lorentz force is the name of this opposite force. There is a consequent consequence of fluid flow retardation. There is a deceleration in the velocity as a result. Moreover, a thickening of its boundary layer is observed. Figures 5B–D illustrate how temperature, concentration profile, and motile density tend to grow dramatically along with an increase in M . Figures 5E, F depict the independent effects of magnetic field M on the formation of entropy and the Bejan number. In contrast to Bejan number's effect, entropy creation has risen. The entropy generation

becomes better due to a rise in hostility to big M . Actually, as the Lorentz magnetohydrodynamic body forces grow strong, the rate of heat transmission (temperature gradient) at the wall increases. The fact that $Ns(\eta)$ is a function of temperature gradient causes stronger magnetic field effects to increase $Ns(\eta)$ levels. The Bejan number decreases because viscous effects dominate the heating and mass transfer effect in our situation. Generally, in this plot, in the free stream, far from the stretching sheet, the Bejan number plummets to zero, whereas the maximum Bejan number arises closer to the wall. Based on these data, the $Ns(\eta)$ profile increases and the $Be(\eta)$ profile decreases. Figure 6A displays the performance of the slip parameter over the dimensionless velocity. Here, when the slip parameter is estimated to be larger, the dimensionless velocity curves fall. Figures 6B–D show that $\theta(\eta)$, $\phi(\eta)$, and $\chi(\eta)$ are mounting behavior leading to the slip parameter Υ . Figures A, B manifest the impact of the mixed convection parameter λ on momentum boundary layer $f'(\eta)$ and temperature $\theta(\eta)$, showing that the improve value of λ let the velocity gradient profile fall. In fact, magnifying λ produces a less bouncy force due to this diversity in the velocity of the fluid. In contrast, reducing performance is noted for the temperature profile in Figure 7B. Figure 8A depicts the impact of the Pr on temperature. The Prandtl number governs the thermal pattern in the illustration Pr . The arcs in this diagram demonstrate how the energy profile decreases as Pr increases because the heat conductivity diminishes as Pr increases. A high Pr value indicates poor thermal conductivity, which lowers the thermal boundary layer and, consequently, conduction, resulting in a drop in fluid temperature. Figure 8B illustrates how the Schmidt number affects the concentration profile $\phi(\eta)$. The results of this figure show that when Sc increases, the thickness of the layers and the associated $\phi(\eta)$ also increase. Momentum diffusivity divided by thermal diffusivity gives the Schmidt number. In fact, when Sc increases, momentum diffusivity improves. This is why $\phi(\eta)$ declines. Figures 9A, B show the effect of density on the Lewis number Lb and Peclet number Pe . Restoration in motile density is correlated with increasing levels of the bioconvection Lewis



number Lb . As the Lewis number Lb increases, the microorganism's diffusivity increases, leading to a progressive rise in the fluid's motile density. The thickness of actively moving microorganisms decreases as the Peclet number Pe increases. The Peclet number quantifies the physical relationship between the prolixity of a microbe and its top swimming speed of individual cells. As the Peclet number rises, the rate at which the cell can swim increases. As the Peclet number of bioconvection increases, the density of motile bacteria decreases. The dispersion of motile microorganisms in the nanofluid is reduced in both scenarios with increasing diffusivity.

TABLE 1 Comparison of $f'''(0)$ for A .

A	Ali et al. [52]	Madhu et al. [55]	Current result
0.8	-1.261479	-1.261211	-1.260691
1.2	-1.377850	-1.377625	-1.377710

TABLE 2 Numerical simulation of the skin friction coefficient $-Re_x^{0.5}C_f$.

Parameter				$-Re_x^{0.5}C_f$	
A	M	We	λ	$n = 0.5$	$n = 1.0$
0.1	0.5	0.1	0.1	1.059210	0.996875
0.5		0.1		1.076897	1.029871
1.0	0.5	0.2		1.093914	1.051456
1.5		0.3	0.1	1.135687	1.093247
0.1	0.7	0.3	0.5	1.094578	1.003693
0.5	0.7	0.3		1.112587	1.031456
1.0		0.4	0.5	1.154879	1.091025
1.5		0.5		1.195465	1.152765
0.1	0.9	0.6	1.0	1.125479	1.061945
0.5		0.6		1.165899	1.102791
1.0		0.6	1.0	1.184578	1.153754
1.5	0.9	0.7		1.292145	1.195476
0.1	1.1	0.8	1.5	1.174783	1.094269
0.5	1.3	0.9		1.102547	1.153794
1.0	1.5	0.9		1.235789	1.181745
1.5	1.5	0.9	1.5	1.262144	1.257956

The impact of $Re_x^{1/2}C_f$, $Re_x^{-1/2}Nu_x$, $Re_x^{-1/2}Sh_x$, $Re_x^{-1/2}Nh_x$ versus magnetic parameter (M) and Peclet number (Pe) has been shown in Figures 10A–H for different values [$n = 1.0, n = 1.5$]. Figures 10A–H show skin friction and Nusselt enhancement, whereas Sherwood and motile density decline as the Weissenberg number parameter (We) and the Bioconvection Lewis number rise (Lb).

Table 1 compares the current problem with the published results of Ali et al. [52] and Madhu et al. [55]. In this comparison, the current outcomes present excellent achievement with the existing published results. Table 2 shows the variation C_f with different values A, M, We , and λ for the two cases when $n = 1.0$ and $n = 1.5$. The skin friction is enhanced by enhancing values of A and We . The escalating performance is bigger for the two cases $n = 1.0$ and $n = 1.5$. The numerical simulation for Nu is seen in Table 3 for $n = 1.0$ and $n = 1.5$. Nu is lessened for the larger values of Nb, Nt , and Bi . The Nusselt number is declined for the case of $n = 1.0$ and $n = 1.5$. The influence of flow variables on Sh for two values of $n = 1.0$ and $n = 1.5$ is presented in Table 4, showing that Sh is enhanced for the larger values of $n = 1.0$ and $n = 1.5$. Table 5 discovers that the

TABLE 3 Numerical simulation of the local Nusselt number $Re_x^{-0.5}Nu_x$. $Pr = 2.5, Sc = 0.5$.

Parameter					$Re_x^{-0.5}Nu_x$	
<i>A</i>	<i>Rd</i>	<i>Nb</i>	<i>Nt</i>	<i>Bi</i>	<i>n</i> = 1.0	<i>n</i> = 1.5
1.0	0.5	1.0	1.3	0.1	0.615793	0.594833
	1.0				0.516896	0.537169
	1.5				0.456345	0.479256
	2.0				0.396453	0.496371
2.0	0.5	1.1	1.4	0.2	0.535465	0.573915
	1.0				0.596486	0.523975
	1.5				0.414568	0.469145
	2.0				0.356822	0.409762
3.0	0.5	1.2	1.5	0.4	0.591176	0.535978
	1.0			0.4	0.551978	0.493671
	1.5				0.439165	0.427196
	2.0				0.398121	0.393971
4.0	0.5	1.3	1.6		0.493145	0.497345
	1.0				0.437128	0.456914
	1.5				0.371930	0.409725
	2.0			0.5	0.309153	0.346571

TABLE 4 Numerical simulation of the local Sherwood number $Re_x^{-0.5}Sh_x$. $Pr = 2.5, Sc = 0.5$.

Parameter				$Re_x^{-0.5}Sh_x$	
<i>A</i>	κ	<i>Nt</i>	<i>Nb</i>	<i>n</i> = 1.0	<i>n</i> = 1.5
1.0	0.5	1.0	1.2	0.056978	0.031456
	1.5			0.089231	0.078841
	2	1.2	1.4	0.157895	0.124556
	0.2			0.459612	0.201356
2.0	0.2			0.045789	0.041789
			1.5	0.094578	0.079684
	0.3	1.3		0.154789	0.135461
				0.235841	0.267245
3.0	0.3	1.3	1.6	0.034569	0.045179
				0.091785	0.096548
	0.4			0.174589	0.186145
		1.4		0.257114	0.269674
4.0	0.4	1.5	1.6	0.286745	0.265481
	0.5			0.334789	0.307896
			1.7	0.378913	0.381745
	0.5	1.6		0.423456	0.443679

TABLE 5 Numerical simulation of the motile density microorganisms.

Parameter				$-Re_x^{0.5}Nh_x$	
<i>Pe</i>	<i>Lb</i>	<i>A</i>	<i>Sc</i>	<i>n</i> = 1.0	<i>n</i> = 1.5
0.1	1.0	1.0	0.1	0.461478	0.443971
0.5				0.395789	0.375412
1.0	2.0		0.1	0.368971	0.336971
1.5			0.2	0.319782	0.308715
0.1	3.0	1.5	0.2	0.407812	0.347892
0.5				0.358136	0.224789
1.0	4.0			0.207834	0.157896
1.5			0.2	0.112536	0.114736
0.1	5.0		0.3	0.331401	0.269445
0.5		2.0		0.241789	0.204698
1.0	6.0		0.3	0.204695	0.145698
1.5				0.133541	0.043508
0.1	7.0	2.5	0.4	0.198713	0.167891
0.5				0.147123	0.125789
1.0				0.102369	0.096314
0.5	8.0		0.5	0.056941	0.037558

bigger magnitude of *n* = 1.0 and *n* = 1.5 leads to depreciation with numerous values of *Lb* and *Pe*.

6 Final remarks

This study measured the impact of velocity slip on the erratic flow of a mixed convection MHD tangent hyperbolic nanofluid containing moving microorganisms. The articulated ordinary differential equation and specified boundary conditions generated from the similarity solutions are resolved using the *bvp4c* solver in MATLAB. MATLAB *bvp4c* is time-saving, efficient, durable, fast-converging, and consistent with earlier studies. The effects of a few associated control parameters are highlighted. The physical variables over $f'(\eta), \theta(\eta), \phi(\eta), \chi(\eta), Ns, Be, Cf, Nu, Sh,$ and Nh have been discussed in detail, and the cogency of the numerical results gained in this study is confirmed by relating them with those obtained earlier. The main result is given as follows:

- Boundary-layer thickness augments for temperature, concentration, and density distributions, although the velocity profile decays as an enhancement in *M* due to resistive Lorentz force.
- The velocity profile declines in contrast to the increasing value of the power law index. Since the dimensionless parameter *n* controls how the fluid behaves under shear, as the power index law magnitude rises, more resistance is put up to the fluid velocity, which decreases the flow.

- When the unsteady variable values increase, the temperature profile increases; however, when the Weissenberg number increases, it decreases.
- The microorganism field has diminished due to the change in Pe and Lb .
- Rising the values of Nb reduces the concentration of the nanoparticles because when Nb grows, the particles prefer to cluster closer together. Conversely, an opposite effect is examined in Nt . Actually, thermophoresis is the movement of tiny particles from a hot to a cool area. When the nanoparticles migrate in the presence of a thermal radiation parameter, more particles are introduced to the process.
- At higher quantities of Pr and Sc , temperature and concentration decrease. Actually, the Prandtl number is determined by the thermal diffusivity to momentum diffusivity ratio. Also, the mass diffusivity decreases with increasing Sc , causing the temperature and concentration contour to be smaller.
- Cf , Nu , Sh , and Nh have revealed accelerating and decreasing behavior through dissimilar values of parameters A , M , λ , Bi , Pe , Lb , Nt , Nb , and We .

Data availability statement

The original contributions presented in the study are included in the article/Supplementary Material. Further inquiries can be directed to the corresponding authors.

References

1. Nadeem S, Hussain ST, Changhoon lee, "flow of a williamson fluid over a stretching sheet. *Brazilian J Chem Eng* (2013) 30(03):619–25. July - September.
2. ZakirUllah GZ. Lie group analysis of magnetohydrodynamic tangent hyperbolic fluid flow towards a stretching sheet with slip conditions. *Cite as: Heliyon* (2017) 3: e00443. doi:10.1016/j.heliyon.2017.e00443
3. Hayat T, Ullah I, Alsaedi A, Ahmad B. Modeling tangent hyperbolic nanofluid flow with heat and mass flux conditions. *Eur Phys J Plus* (2017) 132:112. doi:10.1140/epjp/i2017-11369-0
4. Nagendramma V, Leelathnam A, Raju CSK, Shehzad SA, Hussain T. Doubly stratified MHD tangent hyperbolic nanofluid flow due to permeable stretched cylinder. *Res Phys* (2018) 9:23–32. doi:10.1016/j.rinp.2018.02.019
5. Geethan Kumar S, Varma SVK, Kiran Kumar RVMSS, Raju CSK, Shehzad SA, Bashir MN. Three-dimensional hydromagnetic convective flow of chemically reactive Williamson fluid with non-uniform heat absorption and generation. *Int J Chem Reactor Eng* (2019).
6. Al-Khaled Khan KSUI. Chemically reactive bioconvection flow of tangent hyperbolic nanofluid with gyrotactic microorganisms and nonlinear thermal radiation. *Heliyon* (2020) 6:e03117. doi:10.1016/j.heliyon.2019.e03117
7. Waqas H, Kafait A, Muhammad T, Farooq U. Numerical study for bio-convection flow of tangent hyperbolic nanofluid over a Riga plate with activation energy. *Alexandria Eng J* (2022) 61:1803–14. doi:10.1016/j.aej.2021.06.068
8. Shafiq A, Lone SA, Sindhu TN, Al-Mdallal QM, Rasool G. Statistical modeling for bioconvective tangent hyperbolic nanofluid towards stretching surface with zero mass flux condition. *Sci Rep* () 11:13869. doi:10.1038/s41598-021-93329-y
9. Ali B, sHussain Naqvi SIR, Habib D, Abdal S. Aligned magnetic and bioconvection effects on tangent hyperbolic nanofluid flow across faster/slower stretching wedge with activation energy: Finite element simulation. *Int J Appl Comput Math* (2021) 7:149. doi:10.1007/s40819-021-01097-0
10. Hussain S, Ahmad F, Ayed H, Malik MY, Waqas H, Al-Sawalha MM, et al. Combined magnetic and porosity effects on flow of time-dependent tangent hyperbolic fluid with nanoparticles and motile gyrotactic microorganism past a wedge with second-order slip. *Case Stud Therm Eng* (2021) 26:100962. doi:10.1016/j.csite.2021.100962
11. Shafiq A, Hammouch Z, Sindhu TN, "Bioconvective MHD flow of tangent hyperbolic nanofluid with newtonian heating," *International Journal of Mechanical*

Author contributions

All authors listed have made a substantial, direct, and intellectual contribution to the work and approved it for publication.

Funding

This study was funded by Prince Sattam Bin Abdulaziz University (Project no. PSAU/2023/R/1444).

Conflict of interest

The authors declare that the research was conducted in the absence of any commercial or financial relationships that could be construed as a potential conflict of interest.

Publisher's note

All claims expressed in this article are solely those of the authors and do not necessarily represent those of their affiliated organizations, or those of the publisher, the editors, and the reviewers. Any product that may be evaluated in this article, or claim that may be made by its manufacturer, is not guaranteed or endorsed by the publisher.

Sciences Volume 133, November 2017, Pages 759–66. doi:10.1016/j.ijmecsci.2017.07.048

12. Ramzan M, Chu YM, Gul H, Kadry S, Yu-Ming C. Role of bioconvection in a three dimensional tangent hyperbolic partially ionized magnetized nanofluid flow with Cattaneo-Christov heat flux and activation energy. *Int Commun Heat Mass Transfer Volume* (2021) 120:104994. bioconvection in a three dimensional tangent hyperbolic partially ionized magnetized nanofluid flow with Cattaneo-Christov heat flux and activation energy doi:10.1016/j.icheatmasstransfer.2020.104994

13. Choi SUS. Enhancing thermal conductivity of fluids with nanoparticles. *Int Mech Eng Cong Exp Asme, FED* (1995) 66:99–105.

14. Bhatti MM, Rashidi MM. Effects of thermo-diffusion and thermal radiation on Williamson nanofluid over a porous shrinking/stretching sheet. *J Mol Liq September* (2016) 21:567–73. doi:10.1016/j.molliq.2016.05.049

15. Hayat T, Muhammad K, Farooq M, Alsaedi A. Melting heat transfer in stagnation point flow of carbon nanotubes towards variable thickness surface. *AIP Adv* (2019) 6015214.

16. Kumar PCM, Kuma CMA. Numerical evaluation of cooling performances of semiconductor using CuO/water nanofluids. *Heliyon* (2019) 5:5e02227. doi:10.1016/j.heliyon.2019.e02227

17. Ijaz M, Ayub M, Khan H. Entropy generation and activation energy mechanism in non-linear radiative flow of Sisko nanofluid: Rotating disk. *Heliyon* (2019) 5:5e01863. doi:10.1016/j.heliyon.2019.e01863

18. Khan SU, Shehzad SA. Brownian movement and thermophoretic aspects in third grade nanofluid over oscillatory moving sheet. *Phys Scr* (2019) 94:94095202. doi:10.1088/1402-4896/ab0661

19. Fayaz H, Nasrin R, Rahim NA, Hasanuzzaman M. Energy and exergy analysis of the PVT system: Effect of nanofluid flow rate. *Solar Energy* (2018) 169:217–30. doi:10.1016/j.solener.2018.05.004

20. Ahmed MF, Khalid M, Ali F, Alduais FS, Al-Bossly A, Saeed A. Second law analysis in Darcy-Forchheimer flow of tangent hyperbolic nanofluid in the presence of gyrotactic microorganisms. *Z Angew Math Mech* (2023) e202200466.

21. Olanrewaju AM, Salawu SO, Olanrewaju PO, Amoo SA. Unsteady radiative magnetohydrodynamic flow and entropy generation of Maxwell nanofluid in a porous medium with Arrhenius chemical kinetic. *Cogent Eng* (2021) 8(1):1942639. doi:10.1080/23311916.2021.1942639

22. Alagumalai A, Qin C, Vimal KEK, Evgeny S, Liu Y, Zhang P, et al. Conceptual analysis framework development to understand barriers of nanofluid commercialization. *Nano Energy* (2022) 92:106736. doi:10.1016/j.nanoen.2021.106736
23. Tayebi T, SattarDogonchi A, Karimi N, Ge-JiLe H, Chamkha AJ, Elmasry Y. “2021, Thermo-economic and entropy generation analyses of magnetic natural convective flow in a nanofluid-filled annular enclosure fitted with fins.” *Sustainable Eng Tech Assessments* 46 (2021): 101274. doi:10.1016/j.seta.2021.101274
24. Chamkha AJ, Dogonchi AS, Ganji DD. MagnetohydrodynamicNanofluid natural convection in a cavity under thermal radiation and shape factor of nanoparticles impacts: A numerical study using cvfem. *Appl Sci* (2018) 8:2396–12. doi:10.3390/app8122396
25. Seyyedi SM, Dogonchi AS, Hashemi-Tilehnoee M, Ganji DD, Chamkha AJ. Second law analysis of magneto-natural convection in a nanofluid filled wavy-hexagonal porous enclosure. *Int J Numer Methods Heat Fluid Flow* (2020) 30:4811–36. 11 (January 1, 2020): 4811–36. doi:10.1108/HFF-11-2019-0845
26. Dogonchi AS, Waqas M, Afshar SR, Seyyedi SM, Hashemi-Tilehnoee M, Chamkha AJ, et al. Investigation of magneto-hydrodynamic fluid squeezed between two parallel disks by considering joule heating, thermal radiation, and adding different nanoparticles. *Int J Numer Methods Heat Fluid Flow* (2019) 30(2):659–80. doi:10.1108/HFF-05-2019-0390
27. Eshaghi S, Farhad I, Sattar Dogonchi A, Chamkha AJ, Mohamed B, Ben H, et al. 2021. “The optimum double diffusive natural convection heat transfer in H-shaped cavity with a baffle inside and a corrugated wall.” *Case Stud Therm Eng* 28 (2021): 101541. doi:10.1016/j.csite.2021.101541
28. Afshar SR, Mishra SR, SattarDogonchi A, Karimi N, Chamkha AJ, Abulkhair H. Dissection of entropy production for the free convection of NEPCMs-filled porous wavy enclosure subject to volumetric heat source/sink. *J Taiwan Inst Chem Eng* (2021) 128: 98–113. doi:10.1016/j.jtice.2021.09.006
29. Akram J, Akbar NS, Monairah A, Tripathi D, “Electroosmotically modulated peristaltic propulsion of TiO₂/10W40 nanofluid in curved microchannel” *International Commun Heat Mass Transfer*, Vol. 136, 106208, doi:10.1016/j.icheatmasstransfer.2022.1062082022, 1062.
30. Maraj EN, Zehra I, Akbar NS, “Rotatory flow of MHD (MoS₂-SiO₂)/H₂O hybrid nanofluid in a vertical channel owing to velocity slip and thermal periodic conditions(MoS₂-SiO₂)/H₂O hybrid nanofluid in a vertical channel owing to velocity slip and thermal periodic conditions.” *Colloids Surf A: Physicochemical Eng Aspects*, Vol. 639, 2022, 128383, doi:10.1016/j.colsurfa.2022.128383
31. Akram J, Akbar NS. Mathematical modeling of Aphron drilling nanofluid driven by electroosmotically modulated peristalsis through a pipe. *Math Model Nat Phenom* (2022) 17:19. doi:10.1051/mmnp/2022012
32. Shah Z, Rooman M, Shutaywi M. Computational analysis of radiative engine oil-based Prandtl–Eyring hybrid nanofluid flow with variable heat transfer using the Cattaneo–Christov heat flux model. *RSC Adv Issue* (2023) 13:3552–60. doi:10.1039/d2ra08197k
33. Asghar A, Chandio AF, Shah Z, Vrinceanu N, Deebani W, Shutaywi M, et al. Magnetized mixed convection hybrid nanofluid with effect of heat generation/absorption and velocity slip condition. *Heliyon* (2023) 9(issue 2):e13189. doi:10.1016/j.heliyon.2023.e13189
34. Akbar NS, Maraj EN, Noor NFM, Habib MB. Exact solutions of an unsteady thermal conductive pressure driven peristaltic transport with temperature – dependent nanofluid viscosity. *Case Stud Therm Eng* (2022) 35:102124. doi:10.1016/j.csite.2022.102124
35. Habib MB, Akbar NS. New trends of nanofluids to combat Staphylococcus aureus in clinical isolates. *J Therm Anal Calorim* (2021) 143:1893–9. doi:10.1007/s10973-020-09502-4
36. Akram J, Akbar NS, Tripathi D, “ Electroosmosis augmented MHD peristaltic transport of SWCNT's suspension in aqueous media.” *J Therm Anal Calorim*, 2022, Vol. 147 Issue 3, p2509-26. doi:10.1007/s10973-021-10562-3
37. Shah Z, Ullah A. Ferrofluid treatment with insertion of electric field inside a porous cavity considering forced convection. *Waves in Random and Complex Media* (2023) 1–19. doi:10.1080/17455030.2023.2169386
38. Tang T-Q, Rooman M, Shah Z, MAVrinceanu N, Racheriu M, “2023, Computational study and characteristics of magnetized gold-blood Oldroyd-B nanofluid flow and heat transfer in stenosis narrow arteries,” *J Magnetism Magn Mater*, Vol. 569, 2023, 170448, doi:10.1016/j.jmmm.2023.170448
39. Khan I, Raja MAZ, Khan MAR, Shoaib M, Islam S, Shah Z. Design of backpropagated intelligent networks for nonlinear second-order lane–emden pantograph delay differential systems. *Arabian J Sci Eng* (2022) 47:1197–210. doi:10.1007/s13369-021-05814-1
40. Saini S, Sharma YD. Double-diffusive bioconvection in a suspension of gyrotactic microorganisms saturated by nanofluid. *Int J Appl Fluid Mech* (2019) 12:271–80. doi:10.29252/jafm.75.253.29097
41. Dhanai R, Rana P, Kumar L. Lie group analysis for bioconvection MHD slip flow and heat transfer of nano fluid over an inclined sheet: Multiple solutions. *J Taiwan Instchem Eng* (2016) 66:283–91. doi:10.1016/j.jtice.2016.07.001
42. Mahdy A. Gyrotactic microorganisms mixed convection nanofluid flow along an isothermal vertical wedge in porous media. *Int J Mech Aero Indus Mechatronmanuf Eng* (2017) 11(4):840–50.
43. Avinash K, Sandeep N, Makinde OD, Animasaun IL. Aligned magnetic field effect on radiativebioconvection flow past a vertical plate with thermophoresis and Brownian motion. *Defect Diffus Forum* (2017) 377:127–40. doi:10.4028/www.scientific.net/ddf.377.127
44. Makinde OD, Animasaun IL. Thermophoresis and Brownian motion effects on MHD bioconvection of nanofluid with non-linear thermal radiation and quartic chemical reaction past an upper horizontal surface of a paraboloid of revolution. *J Mol Liq* (2016) 21:733–43. doi:10.1016/j.molliq.2016.06.047
45. Khan WA, Makinde OD, Khan ZH. MHD boundary layer flow of a nanofluid containing gyrotactic microorganisms past a vertical plate with Navier slip. *Int J Heat Mass Transf* (2014) 74:285–91. doi:10.1016/j.ijheatmasstransfer.2014.03.026
46. Mutuku WN, Makinde OD. Hydromagnetic bioconvection of nanofluid over a permeable vertical plate due to gyrotactic microorganisms. *Comput Fluids* (2014) 95: 88–97. doi:10.1016/j.compfluid.2014.02.0262014
47. Khan WA, Makinde OD. MHD nanofluidbioconvection due to gyrotactic microorganisms over a convectively heat stretching sheet. *Int J Therm Sci* (2014) 81: 118–24. doi:10.1016/j.ijthermalsci.2014.03.009
48. Shafiq A, Sindhu T, Masood Khalique C. Numerical investigation and sensitivity analysis on bioconvective tangent hyperbolic nanofluid flow towards stretching surface by response surface methodology. *Alexandria Eng J* (2020) 59(6):4533–48. doi:10.1016/j.aej.2020.08.007
49. Atif SM, Khan WA, Abbas M, Rashid U. BioconvectionMagnetohydrodynamic tangent hyperbolic nanofluid flow with quartic chemical reaction past a paraboloid surface. *Comput Model Eng Sci* (2022) 130(1):205–20. doi:10.32604/cmesci.2022.017304
50. Ashraf MZ, Rehman SU, Farid S, Hussein AK, Ali B, Shah NA, et al. Insight into significance of bioconvection on MHD tangent hyperbolic nanofluid flow of irregular thickness across a slender elastic surface. *Mathematics* (2022) 10:2592. doi:10.3390/math10152592
51. Reddy CS, Ali F, Al-Farhany K, Sridhar W. Numerical analysis of gyrotactic microorganisms in MHDradiative Eyring–Powell nanofluid across a static/movingwedge with Soret and Dufour effects. *Z Angew Math Mech* (2022) 102: e202100459. doi:10.1002/zamm.202100459
52. Ali F, Padmavathi T, Hemalatha B. Entropy minimization in Darcy Forchheimer on Sutterbynano fluid past a stretching surface with swimming of gyrotactic microorganisms. *Waves in Random and Complex Media* (2022) 1–24. doi:10.1080/17455030.2022.2112635
53. Ali F, Reddy CS, Summayya N, Ahmed MF. Effect of nonlinear thermal radiation on unsteady MHD flow of Maxwell nanofluid over a porous vertical sheet with chemical reaction. *Heat Transfer* (2021) 50:8259–79. doi:10.1002/hjt.22276
54. Zhao T, Khan MR, Chu Y, Issakhov A, Ali R, Khan S. Entropy generation approach with heat and mass transfer in magnetohydrodynamic stagnation point flow of a tangent hyperbolic nanofluid. *Appl Maths Mech* (2021) 42:1205–18. doi:10.1007/s10483-021-2759-5
- Madhu, M, Kishan, N, and Chamkha, AJ. Unsteady flow of a Maxwell nanofluid over a stretching surface in the presence of magnetohydrodynamic and thermal radiation effects. *Purpul Power Res* (2015) 6:31–40. doi:10.1016/j.jprr.2017.01.002

Nomenclature

A unsteady parameter (dimensionless)	R_b bioconvection Rayleigh number (dimensionless)
B magnetic field strength ($kg\,s^{-2}A^{-1}$)	Nr nanoparticle concentration (dimensionless)
\bar{C} nanoparticle volume fraction (dimensionless)	U_w stretching sheet velocity (ms^{-1})
\bar{C}_{f_x} skin-friction coefficient (dimensionless)	(\vec{u}, \vec{v}) velocity components (ms^{-1})
\bar{C}_p specific heat ($JKg^{-1}K^{-1}$)	We Weissenberg number (dimensionless)
λ mixed convective parameter (dimensionless)	(\vec{x}) direction along the sheet (m)
D_B coefficient of Brownian diffusion (m^2s^{-1})	(\vec{y}) direction normal to the sheet (m)
D_T coefficient of thermophoresis diffusion (m^2s^{-1})	Υ slip parameter (dimensionless)
D_m microorganism diffusion coefficient (m^2s^{-1})	Bi Biot number (dimensionless)
M magnetic field parameter (dimensionless)	$h(t)$ coefficient of heat transfer ($Wm^{-2}k^{-1}$)
\bar{n} power-law index (dimensionless)	N_s entropy generation (dimensionless)
N_b motion of Brownian parameter (dimensionless)	Be Bejan number (dimensionless)
N_t parameter of thermophoresis (dimensionless)	C stretching parameter (S^{-1})
Nu_x local Nusselt number (dimensionless)	Rd radiation parameter (dimensionless)
Pr Prandtl number (dimensionless)	Greeks
Re_x local Reynolds number (dimensionless)	Γ time constant (sec)
Sc Schmidt number (dimensionless)	ψ stream function (dimensionless)
Sh_x local Sherwood number (dimensionless)	ϕ dimensionless concentration (dimensionless)
\bar{T} temperature (K)	ρ_f density of fluid (Kgm^{-3})
\bar{T}_w temperature at the wall (K)	ρ_p density of particles (Kgm^{-3})
\bar{T}_∞ ambient fluid temperature (K)	Γ time material constant
N microorganism profile (dimensionless)	θ dimensionless temperature (dimensionless)
N_w surface concentration of microorganisms (kgm^{-3})	η similarity variable
N_∞ ambient concentration of microorganisms (kgm^{-3})	α thermal diffusivity (m^2s^{-1})
W_c maximum cell swimming speed (ms^{-1})	$(\rho_c)_f$ heat capacity of fluid (JK^{-1})
Pe Peclet number (dimensionless)	$(\rho_c)_p$ effective heat capacity of the nanoparticle material (JK^{-1})
Lb bioconvection Lewis number (dimensionless)	β volume expansion coefficient (K^{-1})
S_g local volumetric entropy generation rate ($WK^{-1}m^{-3}$)	τ_w wall shearing stress
t time (s)	σ electrical conductivity ($S^3m^2kg^{-1}$)
	ν kinematic viscosity (m^2s^{-1})